Origin and development of uniparental and polyploid blastomeres

Yan Zhao[1,6,7], Andrea Fernández-Montoro[2,7], Greet Peeters[1], Tatjana Jatsenko[1], Tine De Coster[2], Daniel Angel-Velez[2,3], Thomas Lefevre[4], Thierry Voet[4,5], Olga Tšuiko[1], Ants Kurg[6], Katrien Smits[2], Ann Van Soom[2], Joris Robert Vermeesch[1]

[1]Laboratory for Cytogenetics and Genome Research, Department of Human Genetics, KU Leuven, 3000 Leuven, Belgium

[2]Department of Internal Medicine, Reproduction, and Population Medicine - Ghent University, 9820, Merelbeke, Belgium.

[3]Research Group in Animal Sciences – INCA-CES, Universidad CES, 050021 Medellin, Colombia

[4]Laboratory of Reproductive Genomics, Department of Human Genetics, KU Leuven, 3000 Leuven, Belgium

[5]KU Leuven Institute for Single Cell Omics (LISCO), University of Leuven, KU Leuven, Leuven, Belgium

[6]Department of Biotechnology, Institute of Molecular and Cell Biology, University of Tartu, 51010, Tartu, Estonia

[7]These authors contributed equally

Corresponding author: Joris.Vermeesch@KULeuven.be

Abstract

Whole-genome (WG) abnormalities, such as uniparental diploidy and triploidy, cause fetal death. Occasionally, they coexist with biparental diploid cells in live births. Understanding the origin and early development of WG abnormal blastomeres is crucial for explaining the formation of androgenotes, gynogenotes, triploidy, chimerism, and mixoploidy. By haplotyping 118 blastomeres from first cleavages, we identified various mechanisms of heterogoneic divisions that lead to WG abnormal blastomeres or their coexistence with normal blastomeres in both multipolar and bipolar cleaving zygotes. After culturing the totipotent blastomeres to three preimplantation stages and performing transcriptome profiling on over 600 cells, we discovered that stress responses contribute to developmental impairment in WG abnormal cells, resulting in either cell arrest or blastocyst formation. Some first-cleavage-derived WG abnormal blastomeres can survive early development and progress to blastocysts. Their potential dominance in preimplantation embryos represents an overlooked cause of abnormal development. Haplotype based screening could further increase pregnancy rates.

Introduction

Chromosomal abnormalities are common during human development, especially in the preimplantation phase(Hassold et al., 1980; Hassold and Hunt, 2001; Vanneste et al., 2009). One notable category of chromosome abnormalities are whole-genome (WG) anomalies(Masset et al., 2021). Embryos bearing WG abnormalities contain abnormal

levels of parental genomes rather than the normal diploid constellation with one maternal and one paternal haploid genome. For instance, uniparental haploid or diploid embryos carry only chromosomes from a single parent, while triploid embryos contain an additional haploid set of chromosomes from one of the parents. Constitutional WG anomalies are generally lethal during the embryonic stage. Triploidy occurs in approximately 1% of all conceptuses, contributing to around 10% of all spontaneous abortions(Hassold et al., 1980; Zaragoza et al., 2000) with extremely rare live born cases surviving less than a year(Sherard et al., 1986). Complete and partial hydatidiform moles, occurring at rates of 1 in 1000 and 3 in 1000 pregnancies respectively, are primarily androgenetic diploid and diandric triploid, respectively(Seckl et al., 2010). Mosaic forms with coexistence of normal cells can result in rare cases of live birth. For example, gynogenetic and androgenetic chimerism (coexistence of uniparental and normal cells) and diploid/triploid mixoploidy (coexistence of triploid and normal cells) have been reported in live-born individuals with congenital abnormalities(Madan, 2020). As a model organism with a developmental process and an aneuploidy profile similar to that of humans(Hansen, 2010; Santos et al., 2014; Tšuiko et al., 2017), WG abnormalities have also been identified at various stages during bovine development(De Coster et al., 2022; Destouni et al., 2016; Dunn et al., 1970; Meinecke et al., 2003; Tšuiko et al., 2017).

Several models have been proposed to explain the mechanistic origins of WG abnormalities in embryos(Masset et al., 2021). These include dispermy or diploid oocytes leading to triploidy, as well as parthenogenetic division of the oocyte or

fertilization of an 'empty' egg resulting in uniparental embryos. While these models explain the origin of triploid or uniparental embryos, they are limited by the deduction from surviving cells at later developmental stages. Additionally, the mechanistic origins of chimerism and mixoploidy remain speculative(Madan, 2020; Masset et al., 2021). Since all body cells stem from a single zygote, diverse WG abnormalities observed during the late developmental stages are likely the result of irregular zygotic cleavages. Our recent study with bovine *in vitro* fertilized embryos provides direct evidence of a non-canonical first zygotic division as the mechanistic origin of cell lines exhibiting WG abnormalities(De Coster et al., 2022), which we termed "heterogoneic division". This specialized division involves the segregation of entire parental genomes into distinct blastomeres, often triggered by polyspermy and occurring concurrently with multipolar zygotic division. Embryos following heterogoneic division typically contain blastomeres with diverse chromosomal constitutions, including biparental diploid, polyploid, and uniparental blastomeres, resembling those identified in chimeric and mixoploid individuals. Such cleavage involving WG segregation errors has also been reported in *in vitro* human and non-human primate embryos(Daughtry et al., 2019; Ottolini et al., 2017).

Heterogoneic division, as the natural origin of blastomeres with WG abnormalities, represents a fundamental yet underexplored aspect of embryo development. While research on preimplantation embryo development often focuses on aneuploidies and their implications(Fernandez Gallardo et al., 2023; Fragouli et al., 2013; Tšuiko et al., 2021), there has been a lack of investigation into the developmental trajectory of

spontaneously arising blastomeres carrying WG abnormalities. Examining the subsequent development of blastomeres following both heterogoneic and normal first zygotic divisions will provide valuable insights into the developmental disparities between blastomeres with WG abnormalities and normal blastomeres. Such insights are essential for advancing our understanding of the mechanistic origins of triploidy, moles, chimerism, and mixoploidy identified late during development, and will guide genetic testing and embryo selection strategies regarding WG abnormalities.

Here, we explored the genome constitution and developmental potential of individual blastomeres resulting from both bi- and multipolar first zygotic divisions. Through haplotyping of 118 blastomere outgrowths collected at three preimplantation stages, we demonstrated that uniparental and polyploid blastomeres arise from both multipolar and bipolar cleaving zygotes and exhibit a reduced blastocyst rate. Along with single-cell transcriptome analysis of 446 transcriptomes from 124 blastomere outgrowths, we observed impaired transcriptomic development in blastomere outgrowths carrying WG abnormalities, starting from major embryonic genome activation (EGA). This impaired development is attributed to stress responses induced in blastomere outgrowths with WG abnormalities during EGA. Despite these challenges, some blastomere outgrowths with WG abnormalities successfully managed this stress period and progressed to the blastocyst stage, underscoring their potential significant role in abnormal embryo development.

Results

Whole-genome segregation errors occur in multipolar and bipolar first cleavages

To investigate the developmental program of gynogenetic/androgenetic and polyploid blastomeres following spontaneous heterogoneic division, we exploited the totipotency of blastomeres from early cleavage-stage embryos(Johnson et al., 1995; Willadsen, 1980). Daughter blastomeres from 17 bipolar and 35 multipolar cleaved embryos were dissected and individually cultured to either day 2 (T1, 72 hours post fertilization (hpf), 4-6 cell stage), day 4 (T2, 121 hpf, 4-12 cell stage), or day 6 (T3, 170 hpf, blastocyst stage) post blastomere splitting, respectively (**Fig. 1**).

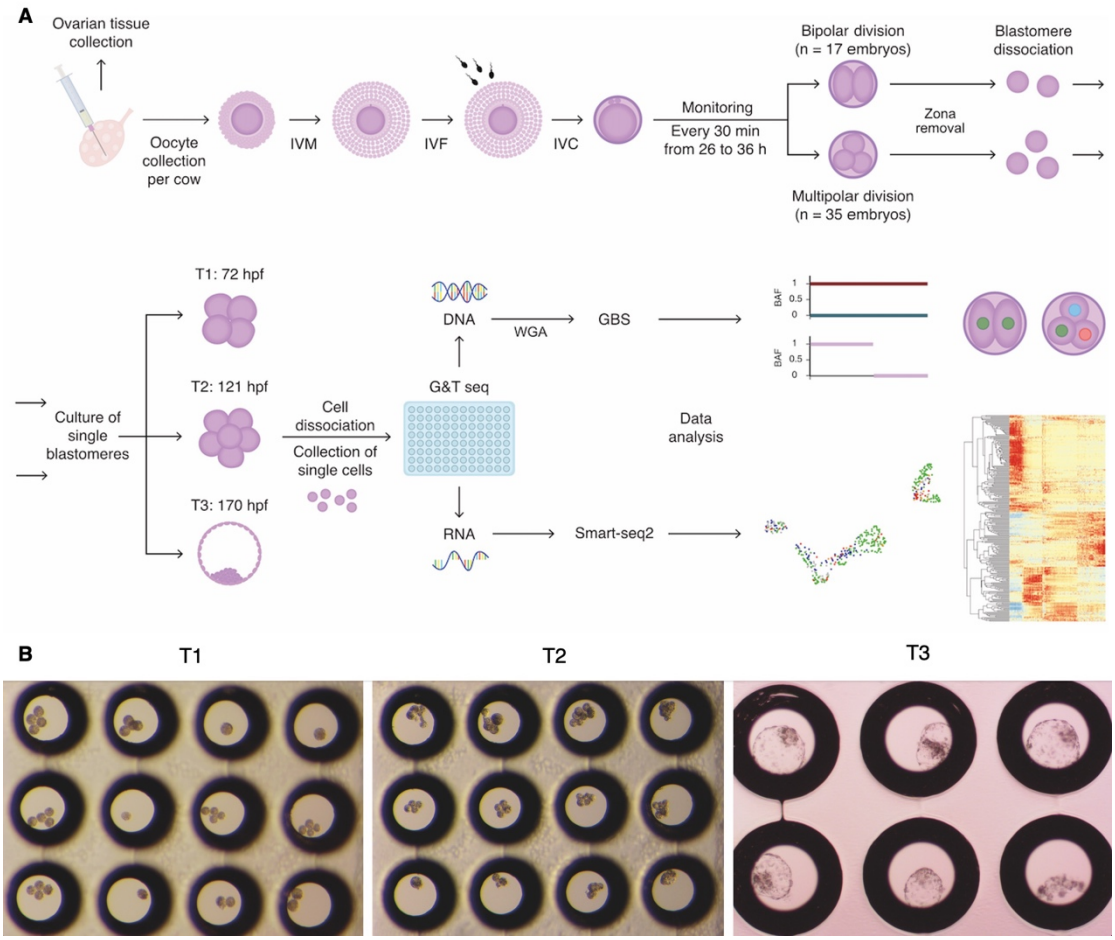

Figure 1. Experimental setup. (A) Diagram illustrating the experimental design. Bovine embryos were created and cultured *in vitro*. After the first zygotic division, blastomeres were

dissected and cultured to three preimplantation timepoints. Blastomere outgrowths were subsequently collected and dissected into single cells. Each dissected cell underwent genome and transcriptome separation followed by sequencing. Genome data were used for haplotyping and copy number profiling, while transcriptome data were used for gene expression analysis. Genome and transcriptome sequencing (G&T-seq): Protocol for isolating poly(A) RNA and genomic DNA from single cells. Genotyping-by-sequencing (GBS): Sequencing-based protocol for genome-wide haplotyping and copy number profiling. (B) Example images of blastomere outgrowths collected at T1, T2, and T3, respectively.

To determine the chromosomal constitution of the blastomeres in culture, we performed genome-wide haplotyping and copy number profiling on cells derived from blastomere outgrowths using genotyping-by-sequencing (GBS) (Masset et al., 2022) (**Fig. 1**). We successfully inferred the chromosomal constitution for all cultured blastomeres in 31 embryos and a subset of cultured blastomeres in 12 embryos, totally getting the chromosomal constitution of 118 blastomeres in culture (**Fig. 2A,B; Supplemental Tables S1,S2**). Among these, 45% (n=53) were identified as biparental diploid, while 41% (n=48) exhibited WG abnormalities, including 35 androgenetic, 9 gynogenetic, 3 diandric triploid, and 1 triandric tetraploid blastomeres. Additionally, 14% (n=17) of the blastomeres in culture with inferred chromosomal constitution were found to be anuclear. All anuclear blastomeres and the majority (96%, 46 out of 48) of blastomeres with WG abnormalities originated from embryos undergoing multipolar first cleavage (**Fig. 2B; Supplemental Table S1**).

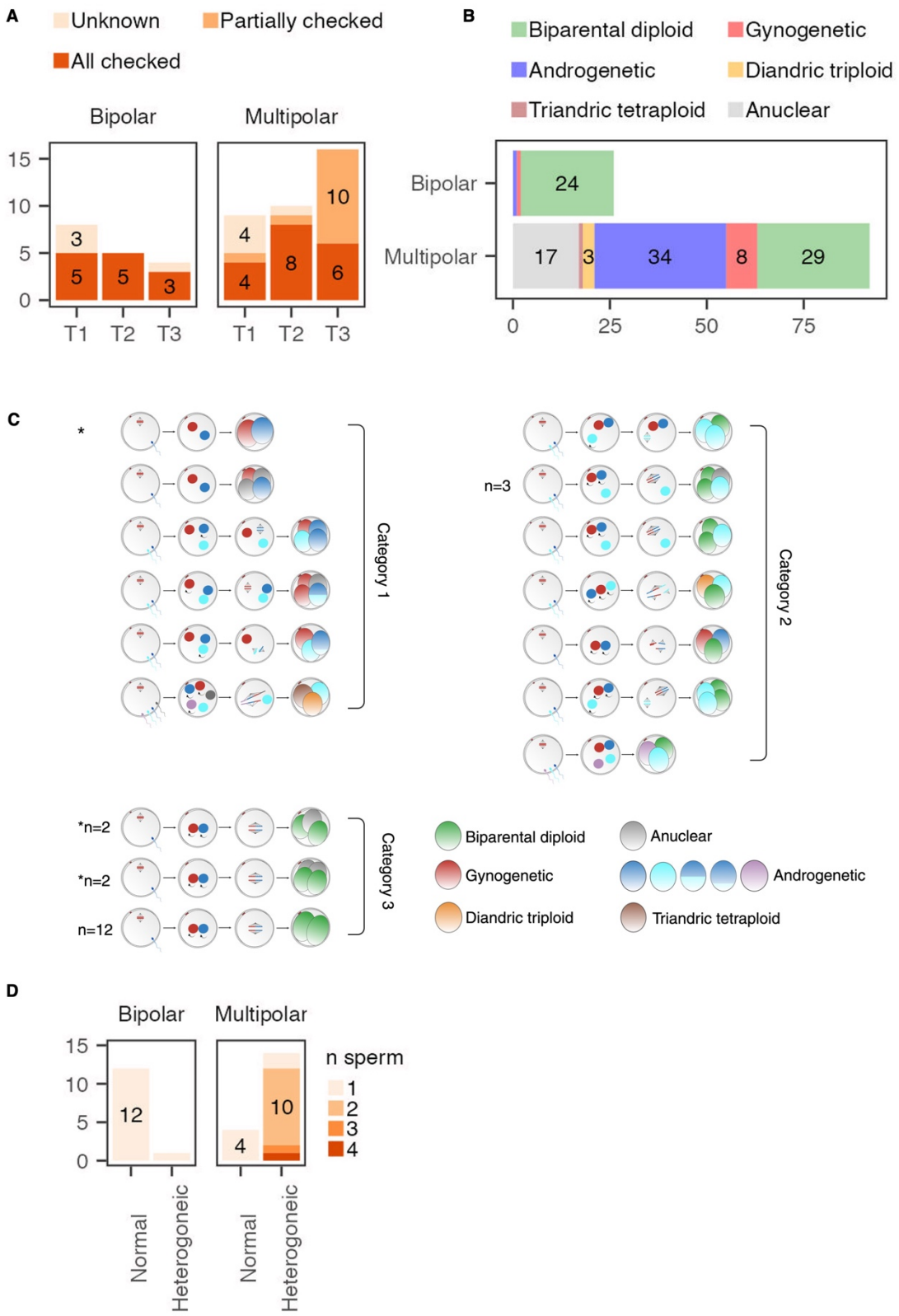

Figure 2. Whole-genome segregation errors occur in multipolar and bipolar first cleavages. (A) Numbers of bipolar and multipolar cleaving embryos used for each blastomere culturing timepoint, categorized based on the completeness of embryo-derived blastomere outgrowth haplotyping: fully haplotyped (All checked), partially haplotyped (Partial), or not haplotyped (Unknown). (B) The inferred chromosomal constitution of 118 blastomeres in culture. (C) Three

categories of genome segregation patterns identified during the first cleavage. In the oocyte being fertilized, the second meiotic division is depicted, along with the likely number of sperms fertilizing the embryo as deduced from the haplotypes. The arrows surrounding the pronuclei indicate replication occurred. During the first cleavage, spindles segregating the sister chromatids are shown. In the absence of a spindle, the genome is extruded. Numbers are given for patterns that occurred more than once. * in category 1 indicates the one embryo with bipolar first cleavage and WG segregation error. * in category 3 indicates the four embryos with multipolar first cleavage and without WG segregation error. For androgenetic blastomeres, different colors indicate genetic material from different sperm. (D) Chromosomal segregation patterns for embryos with bipolar or multipolar first cleavage and the inferred number of sperm that fertilized the egg. Normal: Zygote cleaved without WG segregation error. Heterogoneic: Zygote cleaved with WG segregation error. Bipolar and multipolar refer to embryos undergoing either bipolar or multipolar first cleavage, respectively.

For the 31 fully checked embryos, genome composition of all cultured blastomeres allowed us to reconstruct genome segregation patterns during the first cleavage. We observed three broad categories of genome segregation patterns during the first cleavage (**Fig. 2C; Supplemental Table S1**). Category 1 contains 6 embryos with all blastomeres harboring WG abnormalities. Category 2 comprises 9 embryos with a mixture of blastomeres, some with WG abnormalities and others being biparental diploid. Category 3 consists of 16 embryos with only biparental diploid blastomeres. The four multipolar cleaving zygotes in this category also produced anuclear cells. Among the 31 fully examined embryos, 78% (14 out of 18) of those with multipolar first cleavage demonstrated heterogoneic division, while only 8% (1 out of 13) of embryos with bipolar first cleavage showed WG segregation errors (p=0.00048) (**Fig. 2C**), confirming the enrichment of heterogoneic division in multipolar cleaving zygotes(De Coster et al., 2022). Furthermore, the high frequency of polyspermic conceptions in embryos undergoing multipolar first zygotic division and exhibiting WG segregation errors(De Coster et al., 2022) was validated, with 86% (12 out of 14) of these embryos

173 inferred to be fertilized by more than one sperm. In contrast, all other embryos with
174 bipolar first cleavage or with multipolar first cleavage but without WG segregation
175 errors were inferred to be fertilized by a single sperm (**Fig. 2D**). Only 10% (1 out of 10)
176 of dispermic embryos give rise to triploid blastomeres, which is consistent with previous
177 observations that dispermic fertilization seldom leads to triploid development(De
178 Coster et al., 2022; Kola et al., 1987). Most of the observed mechanisms driving
179 heterogoneic division align with those from our previous study(De Coster et al., 2022;
180 Destouni et al., 2016). Among the 15 embryos undergoing heterogoneic division, 10
181 were inferred to involve the extrusion of paternal pronuclei into separate cells, 4 likely
182 involved an independent spindle separating paternal or maternal chromosomes, 2
183 likely involved a tripolar spindle, and 1 likely involved double spindles (**Fig. 2C**).

184 Interestingly, two novel genome segregation mechanisms were identified. Firstly, within
185 category 1, we observed an embryo undergoing bipolar first cleavage, yet exhibiting
186 heterogoneic division (**Fig. 2C**). The most plausible explanation is that the two parental
187 zygotic spindles failed to align and instead segregated into distinct blastomeres. Hence,
188 genome-wide segregation errors are not confined to multipolar cleavers. Additionally,
189 within category 3, we identified four embryos undergoing multipolar first cleavage, yet
190 exhibiting normal genome segregation. Specifically, two biparental diploid blastomeres
191 were generated alongside one or two anuclear cells (**Fig. 2C**). These findings suggest
192 that bipolar first cleavage does not always ensure normal genome segregation, and
193 multipolar first cleavage does not inevitably result in WG or chromosomal segregation
194 errors.

195 **Blastomeres with whole-genome abnormalities can reach blastocyst stage**
196 **despite impaired developmental potential**

197 To investigate the developmental potential of heterogoneic division-derived
198 blastomeres with WG abnormalities, we compared the developmental stage of the 53
199 biparental diploid blastomere outgrowths and 48 blastomere outgrowths with WG
200 abnormalities at the time of outgrowth collection (**Fig. 3A,B)**. We observed impaired
201 development for blastomeres with WG abnormalities compared to biparental diploid
202 blastomeres at T3, with 80% (12 out of 15) of biparental diploid blastomere outgrowths
203 developing to blastocysts, while only 21% (6 out of 28) of blastomere outgrowths with
204 WG abnormalities reached this stage (p=0.0016) (**Fig. 3B,C**).

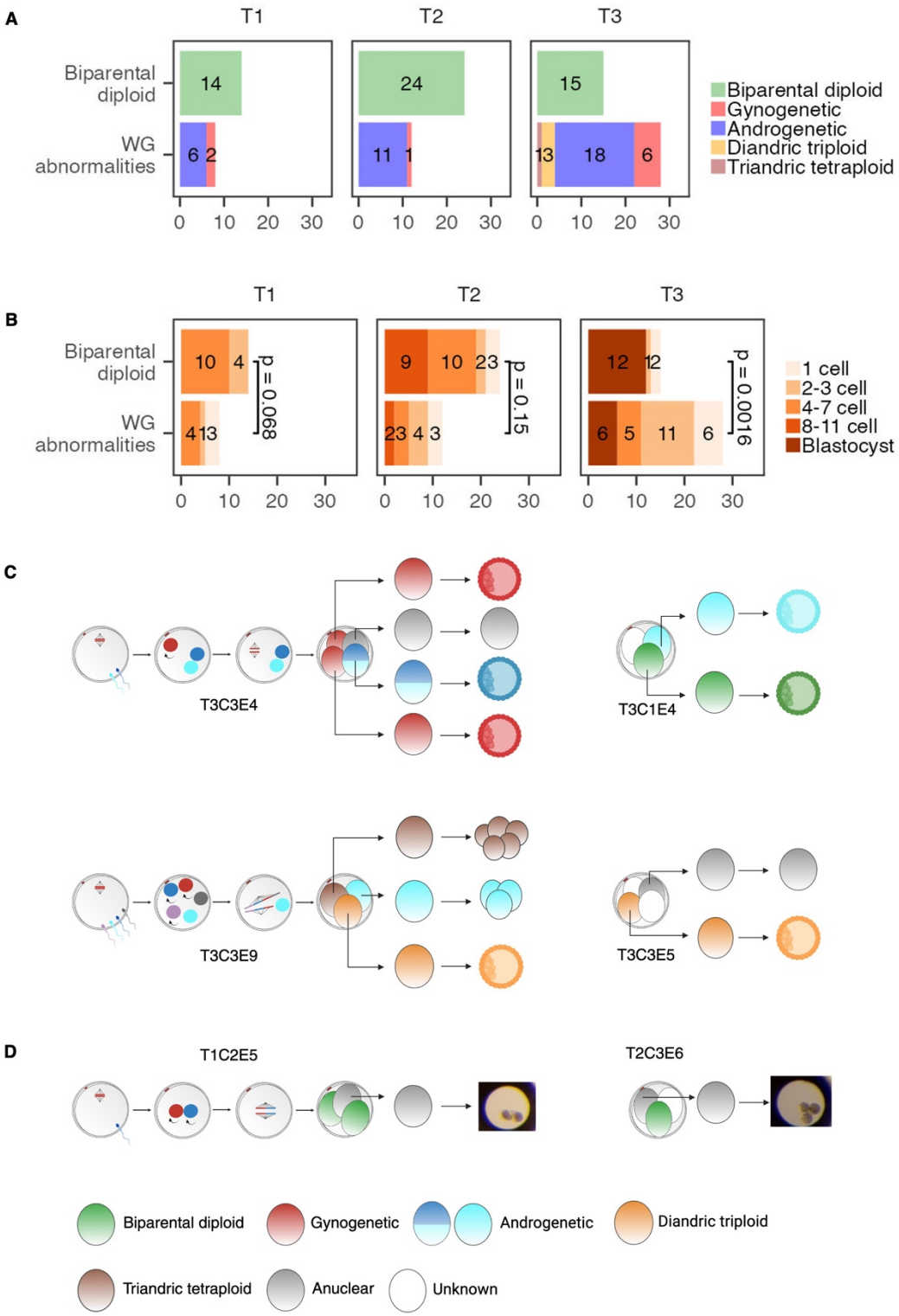

Figure 3. Blastomeres with whole-genome abnormalities can reach blastocyst stage despite impaired developmental potential. (A) Distribution of 53 biparental diploid blastomere outgrowths and 48 blastomere outgrowths with WG abnormalities across different timepoints of outgrowth collection. (B) Developmental stage comparison of biparental diploid blastomere outgrowths and blastomeres outgrowths with WG abnormalities in (A). (C) Schematic representation of the six blastomere outgrowths with WG abnormalities that reached the blastocyst stage at T3, along with their sibling blastomere outgrowths and original embryos. (D)

Images of the two cleaved anuclear blastomere outgrowths and schematic diagrams illustrating the embryos from which they originated. In (C) and (D), the same symbols as in Figure 2C are employed. Fertilization and the first cleavage are not depicted for embryos containing blastomeres with an unknown haplotype (due to sample loss or haplotype failure).

Since aneuploidy is known to affect embryo development, we next evaluated the impact of heterogoneic division on aneuploidy levels in daughter blastomeres. By comparing the aneuploidy spectrum of blastomeres from both normal genome segregation and heterogoneic division, we observed a lower proportion of euploid blastomeres and a higher proportion of blastomeres with high-level aneuploidy (defined as >10% of autosome regions being aneuploid, with 10% corresponding to two large chromosomes) in blastomeres from heterogoneic division, compared to blastomeres originating from zygotes with normal genome segregation (**Supplemental Fig. S1**). Specifically, for blastomeres with WG abnormalities resulting from heterogoneic division, 32% (10 out of 31) were euploid, while 55% (17 out of 31) displayed high level aneuploidy. In contrast, for blastomeres from normal genome segregation, 56% (18 out of 32) were euploid, and only 3% (1 out of 32) exhibited high level aneuploidy (p=6.3×10^{-6}) (**Supplemental Fig. S1**). Similarly, other studies demonstrated the increased rate of complex chromosomal abnormalities for embryos with multipolar division(Daughtry et al., 2019; Zhan et al., 2016). The association between heterogoneic division and vulnerability to chaotic chromosomal missegregations might be caused by the spindle abnormalities implicated in this process (Chatzimeletiou et al., 2005) **(Fig. 2C**). To control for the effect of aneuploidy on blastomere development, we compared the development of only euploid blastomeres. At T3, all biparental diploid blastomere outgrowths (100%,12 out of 12)

237 reached blastocyst stage, while a much lower proportion (36%, 4 out of 11) of
238 blastomere outgrowths with WG abnormalities reached blastocyst stage (p=0.0013).
239 Additionally, for androgenetic blastomere outgrowths collected at T3, 2 out of 15
240 containing the X chromosome reached the blastocyst stage, while the 3 without the X
241 chromosome did not, indicating that the Y chromosome alone is insufficient for
242 blastocyst formation.

243 The majority of the 17 anuclear blastomeres arrested at the 1-cell stage. However, we
244 identified 2 exceptions: one reached the 2-cell stage at T1, and the other reached the
245 3-cell stage at T2 (**Fig. 3D**), suggesting that the cytoplasmic divisions could occur
246 without a nucleus. Additionally, we identified 16 more anuclear biopsies from 14 non-
247 anuclear blastomere outgrowths at various stages of development, with the majority of
248 the original blastomeres (12 out of 14) from embryos underwent multipolar first
249 cleavage (**Supplemental Table S2**). Hence, the formation of anuclear blastomeres is
250 not restricted to the first zygotic division. To confirm the origin of these empty
251 outgrowths/biopsies, we examined the mitochondrial genotypes for empty biopsies
252 obtained from the same cows. Maternal inheritance of the mitochondrial genome was
253 corroborated by similar mitochondrial genotypes (**Supplemental Table S3**).

254 To conclude, blastomeres with WG abnormalities from heterogoneic division show
255 diminished development. Despite this, certain uniparental/polyploid blastomeres still
256 progress to the blastocyst stage (**Fig. 3C**), indicating their viability during the
257 preimplantation stage and raising concerns about their further development and
258 potential contribution to abnormal pregnancies.

259 **Whole-genome abnormalities do not alter the preimplantation developmental**
260 **program but hinder transcriptomic development**

261 We hypothesized that the impaired development of blastomere outgrowths with WG
262 abnormalities would be reflected in the transcriptomic profiles of constituent cells, with
263 WG abnormalities potentially causing deviations in the preimplantation developmental
264 program. To investigate the effects of WG abnormalities on transcriptomic
265 development, we conducted single-cell transcriptome sequencing on 677 cells derived
266 from collected blastomere outgrowths. Among these, 446 transcriptomes met our
267 quality control criteria, representing cells from 124 blastomere outgrowths derived from
268 49 embryos (**Supplemental Table S2; Methods**). We noted significantly higher
269 fractions of mitochondrial transcripts in cells from blastocyst stage outgrowths
270 compared to cells from other stages, except the 1-cell stage (**Supplemental Fig. S2**).
271 The blastocyst stage cells with high fraction of mitochondrial transcripts were not
272 enriched for cells with WG abnormalities. This finding suggests active mitochondrial
273 gene expression in blastocysts and potential cytoplasmic RNA leakage in arrested 1-
274 cell stage outgrowths. Consistent with our findings, previous studies utilizing PCR
275 analysis have demonstrated a significant increase in mitochondrial transcripts at
276 morula and blastocyst stages across various mammalian species(Ma et al., 2008; May-
277 Panloup et al., 2005; Thundathil et al., 2005).

278 Following dimensionality reduction with Unified Manifold Approximation and Projection
279 (UMAP), single-cell gene expression profiles exhibited a developmental trajectory from
280 T1 to T3 (**Fig. 4A**). Cells with WG abnormalities did not form distinct clusters (**Fig. 4B**).

281 Instead, by checking the expression of marker genes for essential preimplantation
282 stages, we identified clusters corresponding to minor EGA, major EGA, inner cell mass
283 (ICM), and trophectoderm (TE) stages, which we define as the molecular
284 developmental stages of the cells. The cell cluster without EGA (pre-EGA) contained
285 cells arrested before EGA (**Fig. 4C; Supplemental Fig. S3**). Pseudotime analysis with
286 single-cell transcriptome data inferred developmental trajectories pointing to ICM and
287 TE (**Fig. 4D**). These results indicate that transcriptomic changes are mainly driven by
288 the natural developmental program rather than variations in genome constitution,
289 aligning with previous single-cell transcriptome analyses of uniparental(Leng et al.,
290 2019) and aneuploid(Fernandez Gallardo et al., 2023) cells from human
291 preimplantation embryos.

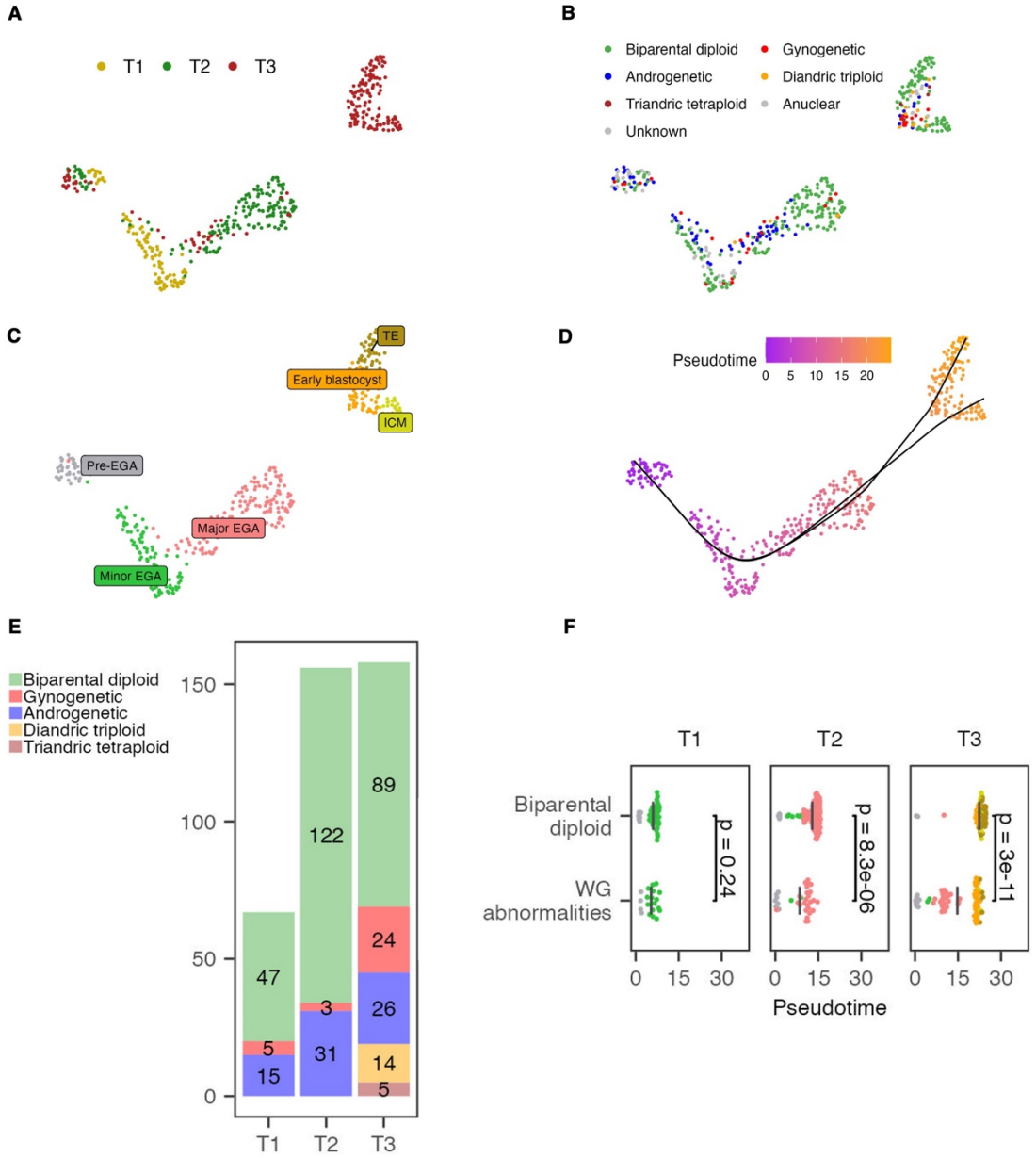

Figure 4. Whole-genome abnormalities do not alter the preimplantation developmental program but hinder transcriptomic development. UMAP for single-cell transcriptome data with cells colored by (A) time of outgrowth collection (B) genome constitution (C) molecular developmental stage indicated by marker genes expression (D) pseudotime value inferred from trajectory analysis. The inferred pseudotime trajectories are indicated by black curved lines on the UMAP. (E) Number of biparental diploid cells and cells with WG abnormalities used for transcriptome analysis for each timepoint. (F) Pseudotime comparison of biparental diploid cells and cells with WG abnormalities at each outgrowth collection timepoint. Each dot represents one cell, with the x-axis indicating its pseudotime value extracted from (D). Cells are colored according to their corresponding molecular developmental stage in (C) using the same color scheme. Vertical grey bars indicate the mean pseudotime value of each group.

We then explored whether the impaired development of blastomeres exhibiting WG

305 abnormalities was reflected in single-cell transcriptome profiles. We characterized the
306 physical age of the cells based on the time of outgrowth collection, while their
307 molecular age was assessed using pseudotime values along the transcriptional
308 trajectory. Compared to cells from biparental diploid outgrowths, those from outgrowths
309 displaying WG abnormalities exhibited impaired development at T2 and T3, as
310 evidenced by their smaller transcriptome-pseudotime ages (**Fig. 4E,F**; $p=4.5\times10^{-5}$ for
311 T2 and $p=4\times10^{-10}$ for T3). This trend persisted when considering only cells inferred to
312 be euploid ($p=0.00026$ for T2 and $p=0.039$ for T3). Our observation indicates the cell-
313 level impaired transcriptomic development of blastomeres with WG abnormalities
314 starting form T2, coinciding with major EGA.

315 Some blastomere outgrowths collected at T2 or T3 did not have the expected number
316 of cells and appeared to be cleaving slower or blocked in their development.
317 Surprisingly, when mapping the transcriptome profiles on the developmental
318 trajectories, we observed that some cells from 1 cell and 2-3 cell stage outgrowths at
319 T3 displayed profiles resembling major EGA, while some cells from 4-7 cell outgrowths
320 exhibited profiles akin to TE or ICM (**Supplemental Fig. S4**). These observations
321 suggest that transcriptomic development can continue in the absence of cell divisions.

322 **Distinct preimplantation cellular states are governed by specific key**
323 **transcription factors**

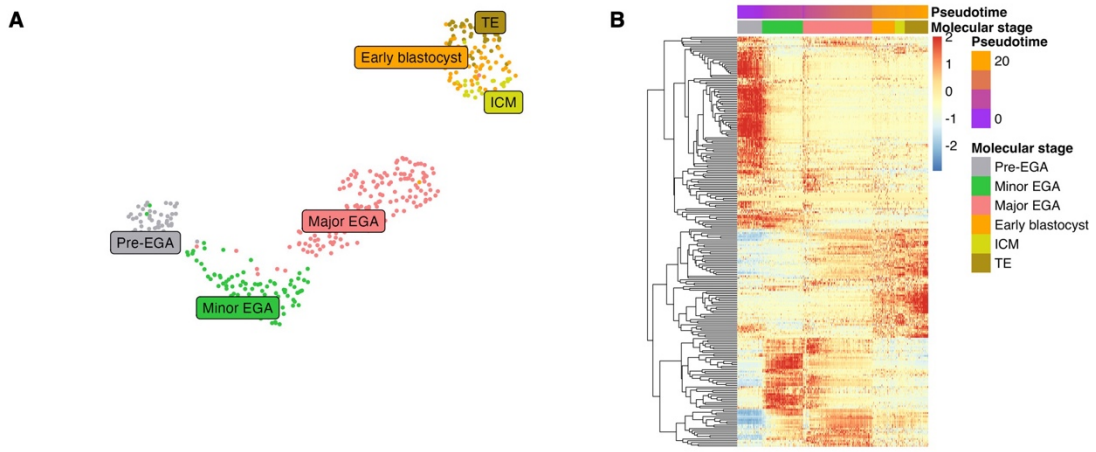

C

Molecular stage	Selected key regulons
Pre-EGA	SIX3, PRDM5, ZBTB43, SMC3, EBF1, HES7
Minor EGA	KLF17, MAX, ZNF143, THAP11, CHD1, IRF3
Major EGA	MITF, ARNT, RARB, HSF1, USF1, BRCA1
Early blastocyst	GATA2, TBX3
ICM	SOX15, NELFB, SREBF1, GATA6, ERF, MAZ
TE	CDX2, TCF7L1, JDP2, JUN, GATA2, GATA3

Figure 5. Distinct preimplantation cellular states are governed by specific key transcription factors. (A) UMAP displaying cell clustering based on regulon activity, with cells colored according to their macular developmental stage as depicted in Figure 4C. (B) Heat map of regulon activity. Each row represents one regulon and each column represent one cell. The plot is generated using rescaled Area Under the Curve (AUC) values, with cells ordered according to their molecular developmental stage and pseudotime values. (C) Key regulons selected for each stage.

Since cells were clustered according to their molecular developmental stage regardless of genome composition, we next aimed to uncover the specific gene regulatory networks (GRNs) shaping cellular identity at each stage. We used pySCENIC to infer GRNs from single-cell RNA-seq data, based on co-expression of TFs and their target genes as well as cis-regulatory motif analysis. This approach identified 237 regulons, each comprising a transcription factor (TF) alongside its predicted target genes. Subsequently, we generated a UMAP visualization based on regulon activity, partitioning cells into distinct regulatory states (**Fig. 5A**). As anticipated,

340 cells belonging to same molecular stage exhibited clustering, indicative of stage-
341 specific regulatory dynamics. To further investigate the coactivity of TF combinations
342 within each stage, we ordered cells based on their molecular stage and pseudotime
343 values on regulon activity heatmap. The resulting plot revealed stage-specific
344 regulatory states characterized by the activation or repression of specific TFs (**Fig. 5B**).
345 We then selected key regulons with both high activity and specificity for each stage
346 (**Fig. 5C; Supplemental Fig. S5; Methods**). Most of the TFs for selected key regulons
347 have been shown to be crucial for embryonic development (**Supplemental Table S4**).
348 For instance, GATA6 has demonstrated significance in the ICM of mouse, bovine, and
349 human embryos(Marsico et al., 2023; Niakan and Eggan, 2013). Similarly, CDX2,
350 GATA2 and GATA3 have been implicated in the TE of mouse, bovine and human
351 embryos(Fernandez Gallardo et al., 2023; Gerri et al., 2020; Home et al., 2017;
352 Nagatomo et al., 2013; Negrón-Pérez et al., 2017; Niakan and Eggan, 2013).
353 Interestingly, for the pre-EGA stage, PRDM5 was identified as a key regulon, reflecting
354 the arrested characteristics of these cells, as this TF is involved in G2/M arrest and
355 apoptosis through suppressing the expression of several oncogenes and antagonizing
356 WNT/β-catenin signaling(Deng and Huang, 2004; Shu et al., 2011). These findings
357 shed light on the combinations of TFs that underlie cell state transitions and cellular
358 identity during bovine preimplantation embryogenesis.

359 **Whole-genome abnormalities induce stress responses during embryonic**
360 **genome activation**

361 Although WG abnormalities did not result in obvious deviations in the preimplantation

developmental program, we hypothesized that the imbalanced parental genome compositions in cells with WG abnormalities could lead to parent-specific gene expression patterns for genes predominantly expressed from only one parent's genome. Furthermore, these WG abnormalities may function as stress stimuli, inducing global transcriptomic changes that ultimately impair the overall developmental potential of cells. To investigate the parental genome-specific effects on gene expression, we compared the gene expression profiles of gynogenetic, androgenetic, and polyploid (diandric triploid and triandric tetraploid) cells to those of biparental diploid cells within each molecular developmental stage. Additionally, to capture the overall effects of WG abnormalities on gene expression, we aggregated all cells with WG abnormalities for combined analyses.

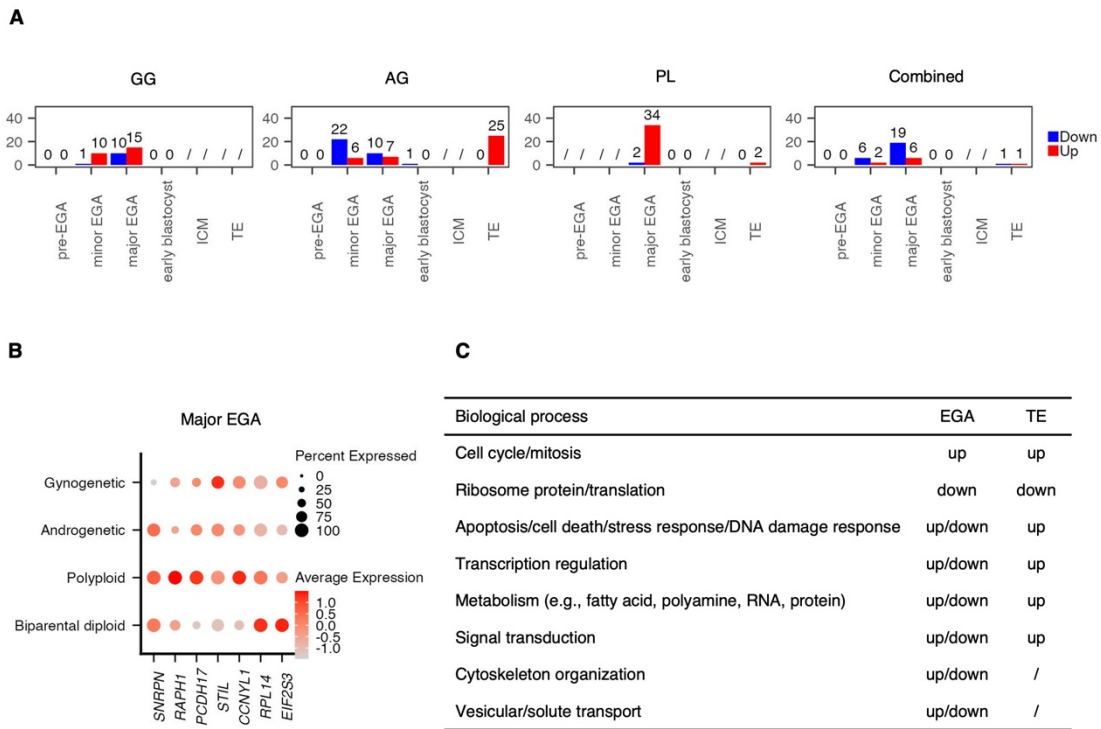

C

Biological process	EGA	TE
Cell cycle/mitosis	up	up
Ribosome protein/translation	down	down
Apoptosis/cell death/stress response/DNA damage response	up/down	up
Transcription regulation	up/down	up
Metabolism (e.g., fatty acid, polyamine, RNA, protein)	up/down	up
Signal transduction	up/down	up
Cytoskeleton organization	up/down	/
Vesicular/solute transport	up/down	/

Figure 6. Whole-genome abnormalities induce stress responses during embryonic genome activation. (A) Numbers of DE genes identified in gynogenetic (GG), androgenetic (AG), polyploid (PL) and combined WG-aberrant cells compared to biparental diploid cells for each

stage. The "/" symbol denotes comparisons not conducted due to insufficient cells. (B) Gene expression dot plot for example DE genes during major EGA. (C) Overall alterations in biological processes reflected by deviations in gene expression. "/" if no DE genes observed.

Differentially expressed (DE) genes were identified from the onset of EGA (**Fig. 6A**), suggesting that WG abnormalities lead to gene expression changes during EGA. Only one DE gene was identified at the early blastocyst stage, indicating a high degree of similarity between normal cells and cells with WG abnormalities just before the first lineage specification. DE genes found in the combined analysis partially overlap with those identified in separate analyses **(Supplemental Fig. S6; Supplemental Table S5)**. Manual functional annotation revealed some parental genome specific effects. We noted the downregulation of the maternally imprinted gene *SNRPN* in gynogenetic cells during major EGA, aligning with its known paternal-specific expression(Lucifero et al., 2006). Furthermore, we identified the up regulation of genes involved in cell adhesion (e.g., *RAPH1, PCDH17*) in polyploid cells during major EGA and at the TE stage (**Fig. 6B; Supplemental Table S5**). This indicates active cell adhesion-related processes, such as compaction in these cells, possibly caused by the additional paternal genome contribution.

Other DE genes observed in uniparental/polyploid cells, as well as those identified through combined analysis, are mainly involved in similar biological processes, indicating global effects of WG abnormalities (**Fig. 6C; Supplemental Table S5**). We observed upregulation of cell cycle/mitosis-related genes (e.g., *STIL*, *CCNYL1*), indicating active preparation for cell cycle progression in cells with WG abnormalities. Meanwhile, we noted downregulation of ribosomal protein genes (e.g., *RPL14*) and

translation initiation factor genes (e.g., *EIF2S3*). It is known that during cellular adaptation to stress stimuli, growth-related genes, including those involved in ribosomes and translation, are typically repressed, prioritizing resources towards stress protection over rapid proliferation(López-Maury et al., 2008). Our observation indicates reduced growth in cells with WG abnormalities as a consequence of the stress response triggered by WG abnormalities. Interestingly, for certain biological processes, DE genes were identified during EGA, leading to either upregulation or downregulation of these processes. No relevant DE genes were found for the early blastocyst stage, while in the TE, no DE genes or only DE genes resulting in upregulated activities of these processes were observed. The biological processes involved include apoptosis, cell death, stress response, DNA damage response, transcription regulation, metabolism, single transduction, cytoskeleton organization and transport **(Fig. 6C; Supplemental Table S5).** This indicates that cells with WG abnormalities adapt to stimuli caused by genome imbalance through transcriptional responses during EGA, involving transient upregulation or downregulation of relevant genes(López-Maury et al., 2008). A quiescent period follows during the early blastocyst stage, while the upregulation of specific genes in TE reflects establishment of new steady-state levels. Additionally, we conducted differential regulon analysis and DE regulons were identified for cells with WG abnormalities only during EGA (**Supplemental Table S5**). Most DE regulons are essential for embryonic development and their bidirectional changes mirror bidirectional gene expression alterations observed in differential gene expression analysis (**Supplemental Table S5**).

422 In summary, we observed parental genome-specific effects induced by WG
423 abnormalities, suggesting distinct roles of the maternal and paternal genomes.
424 Moreover, we identified universal cellular responses to WG abnormalities, marked by
425 active preparation for cell cycle progression alongside reduced cell growth.
426 Bidirectional alterations in specific biological processes and regulons during EGA, and
427 their eventual balance, may dictate whether cells arrest or advance towards the
428 blastocyst stage. Overall, these observed stress responses provide insights into the
429 impaired development cause by WG abnormalities.

430 **Discussion**

431 WG abnormalities are a type of chromosomal error frequently observed in
432 spontaneous abortions(Hassold et al., 1980) and on very rare occasions in a chimeric
433 state in live-born individuals(Madan, 2020). Contrary to its implications in abnormal
434 pregnancy and congenital abnormalities, the proposed origins of such anomalies are
435 deductions from surviving cells at later stages or remain speculative, and their effect
436 on early development remains largely unknown. Here, we provide fundamental
437 insights into the natural emergence and early developmental biology of gynogenetic,
438 androgenetic, and polyploid blastomeres using haplotyping and single-cell
439 transcriptome analysis. We demonstrated the spontaneous occurrence of uniparental
440 and polyploid blastomeres through a non-canonical division during the first zygotic
441 cleavage, which segregates parental genomes into distinct blastomeres. We not only
442 confirmed our previous observation(De Coster et al., 2022) that heterogoneic division
443 mostly coincides with multipolar first cleavage in polyspermic embryos, but also

444 identified, for the first time, heterogoneic division occurring with bipolar first cleavage
445 in normally fertilized embryos. The reduced developmental potential of uniparental and
446 polyploid blastomeres derived from heterogonic division was evidenced by a lower
447 blastocyst rate and a delay in pseudotime values beginning from T2, coinciding with
448 major EGA. Stress responses observed during EGA suggests the cells' efforts to
449 combat fitness challenges induced by aberrant genome composition, with the outcome
450 determining whether they arrest or progress to the blastocyst stage.

451 Although to our knowledge we are the first to explore the development of first-
452 cleavage-derived uniparental and polyploid blastomeres, some studies have examined
453 the preimplantation development of mammalian uniparental embryos. These embryos
454 were generated through various methods, including nuclear manipulation(Hoppe and
455 Illmensee, 1977; Leng et al., 2019; Xu et al., 2021), *in vitro* induction (Hao et al., 2004;
456 Hwang et al., 2020; Ito et al., 1991; Leng et al., 2019; Liu et al., 2002) or natural
457 occurance(Hardy et al., 1989) of parthenogenetic development in unfertilized oocytes,
458 as well as bisection of one-cell fertilized eggs (Tarkowski, 1977). Aligned with the
459 impaired developmental potential observed in blastomeres with WG abnormalities in
460 our study, those studies on preimplantation uniparental embryos have shown a
461 decrease in the morula/blastocyst rate compared to biparental diploid embryos.,
462 alongside poorer morphology and reduced cell count in resulting blastocysts(Hardy et
463 al., 1989; Leng et al., 2019). Several studies have monitored post-implantation
464 development and affirmed the compatibility of diploid uniparental genome constitution
465 with later development. For instance, porcine parthenogenetic fetuses can develop

466 until day 35 with abnormal organ morphologies (Hwang et al., 2020). Additionally, live-
467 born fertile mice have been created via both androgenesis and gynogenesis(Hoppe
468 and Illmensee, 1977). Moreover, diploid gynogenetic cells have been identified in
469 various organs of live-born chimeric mice developed from aggregated chimeric
470 embryos(Ito et al., 1991). These findings are consistent with observations in humans,
471 suggesting that uniparental cell lines are typically selected against during development
472 but can persist until late pregnancy and even be compatible with live birth, raising
473 various concerns. Our study demonstrates that heterogoneic division could serve as a
474 spontaneous origin of uniparental and polyploid cell lines observed during late
475 development.

476 The parental genome specific effects identified in this study correlates with findings
477 from a prior investigation of uniparental human embryos(Leng et al., 2019). As for the
478 stress response observed solely in our study, there are possible causes aside from
479 species-specific effects and sample variations(Xu et al., 2021). The referenced study
480 created diploid gynogenetic and androgenetic embryos through nuclear manipulation
481 and induction of parthenogenesis, respectively. Only embryos demonstrating good
482 morphology and developmental speed were utilized. Only XX and XY androgenetic
483 embryos were included. And their analysis focused exclusively on genes with highly
484 biased expression in gynogenetic or androgenetic embryos. In contrast, our study
485 focused on a broad spectrum of spontaneously occurring WG abnormalities, which
486 frequently exhibit complex aneuploidy and contain either haploid or diploid genome
487 constitutions. While haploidy has been demonstrated to convert frequently to diploidy

488 during development(Ito et al., 1991; Leng et al., 2017; Tarkowski, 1977), both complex
489 aneuploidy and haploidy are known to impact preimplantation development(Liu et al.,
490 2002; McCoy et al., 2015). Additionally, our cohort included androgenetic blastomeres
491 lacking the X chromosome, a condition known to cause embryonic arrest. Finally,
492 rather than focusing solely on genes with highly biased expression in gynogenetic or
493 androgenetic embryos, our study examined the broader impact of WG abnormalities
494 on global gene expression changes. These factors led us to observe EGA as a critical
495 period for embryos with WG abnormalities. During this stage, their constituent cells
496 exhibit stress responses in gene expression, which could determine whether they
497 arrest or successfully progress to the blastocyst stage.

498 We identified anuclear cells from outgrowth at different stages, which is in agreement
499 with previous observations in rhesus(Daughtry et al., 2019) and human embryos(Hardy
500 et al., 1993). Consistent with our previous analysis(De Coster et al., 2022), most of the
501 anuclear blastomeres were identified from blastomere outgrowths following multipolar
502 first cleavage, suggesting a potential association between the first cleavage pattern
503 and the origin of these anuclear cells. In addition, we demonstrate that some of the
504 anuclear cells can cleave without nuclei. Cytoplasmic divisions are generally thought
505 to rely on nuclear divisions and mitotic signals. However, a recent study by Bakshi et
506 al. observed that cytoplasm can compartmentalize, and a rare fraction of the
507 compartments can divide repeatedly without nuclei and independent of mitotic
508 CDK/cyclin complexes during normal drosophila embryogenesis (Bakshi et al., 2023).
509 They showed that this phenomenon is relevant to mitotically delayed nuclei. We

510 hypothesize that a similar mechanism may apply here, with the anuclear cells derived
511 from mother cells containing nuclei with delayed mitosis. These findings collectively
512 underscore the need for further investigation into the detailed mechanisms underlying
513 the presence of anuclear cells in mammalian embryos and their potential roles in
514 embryo development.

515 Insights from this study raise clinical concerns. Firstly, in IVF laboratories, human
516 embryos with two pronuclei (PN) are preferentially selected for transfer(Balaban et al.,
517 2011). We demonstrate here that zygotes with three PN may result in a mixture of
518 biparental diploid and uniparental/polyploid blastomeres. Since the latter are
519 developmentally compromised, the resulting embryo may still develop normally.
520 Secondly, there is a growing trend in many laboratories to monitor embryonic
521 development using time-lapse microscopy and rank embryos based on cleavage
522 kinetics(Balaban et al., 2011; Sigalos et al., 2016; Sugimura et al., 2017, 2012).
523 Embryos with multipolar first cleavage are typically given a low rank. We showed here
524 that 22% of embryos with a multipolar first cleavage exhibited normal, equal division
525 of the genome with additional anuclear cells. It would be unjust to low rank these
526 embryos since they have the potential to lead to healthy babies. Additionally, even
527 though uniparental/polyploid cells are normally generated with multipolar first cleavage,
528 it is not uncommon that biparental diploid blastomeres are generated together, which
529 may gain developmental advantage and lead to normal development. Thirdly, embryos
530 typically ranked high, characterized by a normal pronuclei count and bipolar first
531 cleavage, may still experience WG segregation errors, leading to the generation of

532 solely uniparental cells, posing a potential risk of abnormal pregnancy. Rather than
533 removing or keeping embryos based on apparent abnormalities, it might be better to
534 evaluate the genome constitution of preimplantation embryos and deselect those with
535 WG abnormalities, while retaining those with a normal chromosome count and parental
536 haplotype constitution. Preimplantation genetic testing for aneuploidy (PGT-A) has
537 become a common practice to select embryos with a normal number of chromosomes
538 for transfer. However, the majority of PGT-A tests only measure aneuploidies, with
539 only some measuring the parental haplotype constitution(Coonen et al., 2020). We
540 suggest the use of genotyping/haplotyping together with PGT-A(Masset et al., 2022;
541 Zamani Esteki et al., 2015) to check both chromosome count and parental haplotype
542 constitution and select against WG abnormalities. This approach is likely to further
543 improve the overall IVF success rate(Caroselli et al., 2023).
544 In conclusion, this study provides comprehensive insights into the natural origin and
545 early development of uniparental/polyploid blastomeres. We demonstrated their
546 overall impaired developmental potential, primarily due to stress responses triggered
547 by WG abnormalities during EGA. Blastomeres that successfully navigate through this
548 phase and progress to the blastocyst stage may constitute a significant fraction of
549 embryos and contribute to abnormal development. Our findings underscore the
550 importance of routine screening against embryos bearing WG abnormalities in IVF labs.

551 **Materials and Methods**

552 **Single-cell collection from bovine blastomere outgrowths**

553 *In vitro embryo production*

554 Prior ethical agreement was not necessary. Ovaries from cows raging 4 to 5 years
555 were collected post-mortem in a commercial slaughterhouse. The sperm used for *in*
556 *vitro* fertilization was collected from a 5-years-bull. Standard in vitro procedures were
557 followed to produce bovine embryos (Wydooghe et al., 2014). Briefly, bovine (*Bos*
558 *taurus*) ovaries were collected and processed within 2 h. The ovaries were rinsed three
559 times in warm physiological saline supplemented with 0.25µg/mL kanamycin. Using an
560 18-G needle and a 10-mL syringe, antral follicles (2 – 8 mm diameter) were punctured
561 and kept separately per ovary in 2.5 mL Hepes-Tyrode's albumin-pyruvate-lactate
562 (Hepes-TALP). Using a stereomicroscope, cumulus-oocyte complexes were collected
563 and washed in Hepes-TALP and then in maturation medium (modified bicarbonate-
564 buffered TCM-199 supplemented with 50 ppm gentamicin and 20 ng/mL epidermal
565 growth factor). Cumulus-oocyte complexes were *in vitro* matured per donor in four-well
566 dishes (NuncTM) in 500 µL maturation medium for 22 h at 38.5°C in 5% CO_2 in
567 humidified air. *In vitro* fertilization was performed with frozen-thawed semen from a
568 Holstein-Friesian bull (*Bos taurus*) after selection over a discontinuous 45/90%
569 Percoll® gradient (GE Healthcare Biosciences, Uppsala, Sweden). The mature oocytes
570 were fertilized by incubating them with spermatozoa at a concentration of 1×10^6
571 spermatozoa/mL in IVF–TALP medium enriched with BSA (Sigma A8806; 6 mg/mL)
572 and heparin (20 µg/mL) for 21 hours at 38.5°C, 5% CO_2 in humidified air. After
573 fertilization, the presumed zygotes were vortexed in 2.5 mL HEPES-TALP for 3 minutes
574 to remove the cumulus and sperm cells adhered to the *zona pellucida* and

575 subsequently transferred to 50 µL droplets of synthetic oviductal fluid (SOF), enriched
576 with 4 mg/mL BSA (Sigma A9647), non-essential and essential amino acids (SOFaa),
577 5 µg/mL insulin, 5 µg/mL transferrin, and 5 ng/mL selenium. The droplets were covered
578 with 900 µL paraffin oil (SAGE oil for tissue culture, ART-4008-5P, Cooper Surgical
579 Company). *In vitro* culture was performed at 38.5 °C in 5% CO_2, 5% O_2, and 90% N_2.

580 *Blastomere dissociation and culture*

581 The presumptive zygotes were monitored from 26 to 36 hours post-fertilization (hpf)
582 every 30 minutes to identify a direct cleavage of the zygote into three or four
583 blastomeres (multipolar division) or into two blastomeres (bipolar division).
584 Blastomeres from embryos that cleaved into more than four cells or presented multiple
585 fragments were not processed further. Immediately upon the first division, embryos
586 were washed in Hepes-TALP and treated with 0.1% pronase (protease from *S. griseus*)
587 in TCM-199 to dissolve the *zona pellucida*. Next, the embryos were washed in TCM-
588 199 with 10% FBS and then transferred to Ca^{+2}/Mg^{+2}-free PBS with 0.05% BSA to
589 enhance blastomere dissociation, which was performed using a STRIPPER pipet
590 holder and 170 µm and 135 µm capillaries (Origio, Cooper Surgical, CT, US) in
591 Ca^{+2}/Mg^{+2}-free PBS supplemented with 0.1% polyvinylpyrrolidone (PVP).
592 Subsequently, single blastomeres were washed in culture medium and transferred
593 individually to one well of a Primo VisionTM micro well group culture dish (Vitrolife,
594 Göteborg, Sweden), which contained a total of 16 small wells covered by a 40 µL
595 droplet of culture medium and 3.5 mL paraffin oil. Single blastomeres were cultured at
596 38.5°C in 5% CO_2, 5% O_2, and 90% N_2 until 72, 121 or 170 hpf according to the

experimental design.

Single-cell isolation

For isolation of single cells at 72 hpf, 121 hpf or from blastomeres that did not reach the blastocyst stage at 170 hpf, the outgrowths were transferred to Ca^{+2}/Mg^{+2}-free PBS with 0.1% PVP, and the cells were dissociated mechanically with a STRIPPER pipet holder and 170 µm and 135 µm capillaries (Origio, Cooper Surgical, CT, US). For blastomeres that reached the blastocyst stage at 170 hpf, single-cell isolation was done by incubating the embryos in trypsine-EDTA at 38.5°C, followed by washing in Ca^{+2}/Mg^{+2}-free PBS with 0.1% PVP, pipetting with a STRIPPER pipet holder, and 135 µm and 70 µm capillaries (Origio, Cooper Surgical, CT, US) and micromanipulation with holding (MPH-MED-35, Origio, Cooper Surgical, CT, US) and biopsy (MBB-BP-M-30, Origio, Cooper Surgical, CT, US) pipettes. When single-cell dissociation was not possible, clusters of cells were collected. Single cells from all time points were washed in Ca^{+2}/Mg^{+2}-free PBS with 0.1% PVP before transferring them into a well of a skirted 96-well plate (4ti-0960/C, AZENTA Life Sciences, Bioké, Leiden, The Netherlands) containing 2.5 µL of RLT lysis buffer with a 70 µm capillary (Origio, Cooper Surgical, CT, US) and a STRIPPER pipet holder screwed on 0.5 µL. The collected samples were kept on ice during the whole procedure and then stored at −80°C.

DNA and RNA separation, library preparation and sequencing

Separation of DNA and RNA from single cells

618 The DNA and mRNA from single cells were separated following the genome and
619 transcriptome sequencing (G&T-seq) protocol(Macaulay et al., 2016) on a robotic
620 liquid-handling platform (Microlab STAR Plus, Hamilton). Specifically, the 96-well
621 sample plate was positioned on the robot deck alongside (a) a plate for capturing poly-
622 A mRNAs, containing 10µl per well of Dynabeads® MyOneTM Streptavidin C1 (Thermo
623 Fisher Scientific) bound to biotinylated poly-dT oligos containing the SmartSeq2 primer
624 sequence '5BioTinTEG/ -
625 AAGCAGTGGTATCAACGCAGAGTACTTTTTTTTTTTTTTTTTTTTTTTTTTTTTTVN'
626 (IDT), (b) a plate for washing away DNA from the cell lysate supernatant, containing
627 25µl per well of G&T-wash buffer, and (c) an empty DNA destination plate. First, the
628 cell lysate was mixed with biotinylated poly-dT beads and incubated for 20 min.
629 Subsequently, beads bound to mRNA were pulled down using a low elution magnet
630 (Alpaqua) for 2 min, and the supernatant was transferred to the DNA destination plate.
631 Following this, the beads were subjected to two washes, each with 10µl of G&T wash
632 buffer, and the supernatant was transferred to the DNA destination plate. The DNA
633 destination plate, containing 37.5µl of G&T wash buffer, was then centrifuged for 1 min
634 at 1000g and stored at -80°C.

635 *RNA amplification, library preparation and sequencing*

636 The plate containing poly-A mRNA-bound beads was processed using an adapted
637 SmartSeq2 protocol with 20 PCR cycles. Subsequently, the amplified single-cell cDNA
638 was purified using a 0.8:1 ratio of Agencourt AMPure XP beads (Analis), followed by
639 washing with 80% ethanol and elution in water. Libraries were generated from the

640 amplified cDNA according to the Nextera XT (Illumina) protocol with quarter volumes.
641 These libraries were pooled and sequenced using single-end 50 sequencing on a
642 HiSeq4000 Illumina sequencer, aiming at 1 million reads per sample. For a subset of
643 blastocyst stage single cells, the libraries were resequenced paired-end 150 on a
644 NovaSeq 6000 Illumina sequencer for more reads.

645 *DNA amplification, GBS library preparation and sequencing*

646 For each blastomere outgrowth, DNA from either individual single cell or several cells
647 was used for GBS (with double enzyme restriction) processing. A sibling blastocyst
648 was collected and processed together when available. Whole-genome amplification
649 (WGA) was carried out using the REPLI-g SC kit (Qiagen, Germany) following the
650 manufacturer's guidelines, with variations in reaction volumes (full or half) and an
651 incubation period of 2-3 hours. The DNA separated from the single cells stored in G&T
652 wash buffer (see before), was thawn on ice, centrifuged for 1 min at 1000g, purified
653 with Agencourt AMPure XP beads (Beckman Coulter, USA), eluted in 4 µl of scPBS
654 and processed following the REPLI-g SC kit (Qiagen, Germany) manufacturer's
655 guidelines with an incubation time of 2h. Additionally, bulk DNA was extracted from
656 ovarian tissue of the donor cows (mothers of the respective embryos), semen from the
657 bull (father of the embryos), and blood from the parents of the bull (paternal
658 grandparents of the embryos) using the DNeasy Blood and Tissue kit (Qiagen,
659 Germany).

660 The whole-genome amplified DNA and bulk DNA were subjected to double restriction

661 digestion with 8 units (U) of PstI-HF (R3140S, NEB) and 4U of CviAII (R0640L, NEB)
662 enzymes (New England Biolabs, NEB, USA) combined with adapter ligation using 200-
663 300 ng as an input DNA for each sample. The restriction-ligation reaction was
664 performed in a total reaction volume of 15 µl, with a final concentration of 1X rCutSmart
665 buffer (B6004S, NEB), 1mM ATP (P0756S, NEB) and 160U of T4 DNA Ligase (M0202L,
666 NEB). Next, the double-sided size-selection was performed with Agencourt AMPure
667 XP beads (Beckman Coulter, USA) and 7 cycles of PCR to amplify and barcode size-
668 selected adapter-ligated fragments using Q5 High-Fidelity 2X Master Mix (NEB) and
669 0.5 µM primer mix with the following program. Subsequently, the libraries were purified
670 with Agencourt AMPure XP beads (Beckman Coulter, CA, USA), equimolarly pooled
671 and sequenced paired-end 150 on NovaSeq 6000 Illumina sequencer, with a target of
672 20-30 million reads per sample.

673 **Data analysis**

674 *GBS data processing, haplotyping and aneuploidy profiling*

675 The raw reads were processed using fastp (v0.23.2)(Chen et al., 2018) to trim adaptor
676 sequences, filter out low-quality reads, remove UMI sequences and append them to
677 read names. Next, cutadapt (v 1.18)(Martin, 2011) was applied to select reads that
678 start with the internal barcode and trim off the barcode. Reads were then mapped to
679 bovine reference genome bosTau9 (ARS-UCD1.2) using BWA-MEM (v0.7.17)(Li,
680 2013). Next, UMICollapse(Liu, 2019) was used for collapsing duplicated reads with the
681 same UMI, while accounting for sequencing/PCR errors. Across all samples, we

682 obtained a median of 64 million mapped reads. After UMI deduplication, a median of
683 35 million mapped reads were retained (**Supplemental Table S2**). Variant calling was
684 performed with freebayes (v 1.3.2)(Garrison and Marth, 2012). Initially, variants were
685 called for the parents and phasing reference(s) (parental grandparents or a sibling
686 blastocyst). Subsequently, the identified variants were utilized as input to call variants
687 for each single/multi-cell sample. The called SNVs were converted into bi-allelic calls
688 (e.g., AA, AB, and BB) with B-allele frequency (BAF) values calculated based on allele-
689 specific depth of coverage using a custom R script. The genotype calls and BAFs were
690 then used as input for the siCHILD pipeline (details in the method paper(Zamani Esteki
691 et al., 2015)). In brief, siCHILD performs pedigree-based haplotyping analysis. The
692 parents were first phased using phasing reference(s). Subsequently, for specific
693 combinations of phased parental genotypes, corresponding SNP BAF values of the
694 sample of interest were retrieved and plotted on paternal and maternal haplarithms.
695 Genome-wide parental haplotype inheritance can then be inferred through visual
696 inspection of the genome-wide haplarithm plots.

697 In addition to haplotype information, the R package QDNAseq and custom scripts were
698 applied to BAM files post-deduplication for aneuploidy profiling with a fixed bin size of
699 100kb. To quantify the extent of aneuploidy, the percentage of aneuploid autosomal
700 regions was calculated for each sample. Specifically, bins with a segmentation logR
701 value within $log2(1/2)$) and $\log2(3/2)$ were classified as normal, while all other bins
702 were classified as abnormal. The percentage of aneuploid autosomal regions was
703 calculated by summing up the length of all abnormal bins and dividing it by the size of

704 all autosomes. Samples were categorized based on the percentage of aneuploid
705 autosomal regions: $\leq \%1$ as euploid, 1-5% as low-level aneuploidy, 5-10% as
706 medium-level aneuploidy, and >10% as high-level aneuploidy. To determine
707 chromosome X nullisomy status, the lengths of all bins on chromosome X with a
708 segmentation logR value ≤ -3 were aggregated. The fraction of the chromosome X
709 region exhibiting nullisomy was determined by dividing this sum by the size of
710 chromosome X. Samples with >95% nullisomy in the chromosome X region were
711 classified as chromosome X nullisomy.

712 The haplotype composition and aneuploidy status of each blastomere outgrowth were
713 determined using GBS results from a single-cell/multi-cell sample. A sample was
714 considered anuclear if >60% and >10% of the reads mapped to the mitochondrial
715 genome before and after UMI deduplication, respectively, with empty haplarithm and
716 copy number plots. To infer an outgrowth to be anuclear, each cell in the outgrowth
717 was individually checked and confirmed to be anuclear. To verify the presence of
718 mitochondrial genomes in inferred anuclear biopsies and ascertain their maternal
719 inheritance, we exclusively called variants on the mitochondrial genome across all
720 inferred anuclear biopsies using Freebayes (v1.3.2)(Garrison and Marth, 2012) and
721 compared the called genotypes (**Supplemental Table S3**).

722 *Single-cell RNA sequencing data preprocessing*

723 The raw reads were processed with fastp (v0.23.2)(Chen et al., 2018) to trim adaptor
724 sequences and filter out low-quality reads. Subsequently, the reads were mapped to

725 the bovine reference genome bosTau9 (ARS-UCD1.2) using STAR aligner (v
726 2.7.3)(Dobin et al., 2013) with Ensembl annotations ARS-UCD1.2.105. Next, raw
727 counts per cell were obtained using HTSeq (v 0.9.1)(Anders et al., 2015). Cells with
728 fewer than 200,000 detected molecules or fewer than 2,000 expressed genes were
729 excluded from further analysis, resulting in 446 cells out of 677 passing these quality
730 control thresholds. The retained cells exhibited a median of 862,384 molecules and
731 7,272 genes detected per cell (**Supplemental Table S2**). Counts were then normalized
732 and scaled using R package Seurat (v5.0.1)(Hao et al., 2023).

733 *Cell clustering, cell type identification and trajectory analysis*

734 Cell clustering was performed based on the normalized and scaled transcriptome
735 profiles using UMAP implemented in Seurat (v5.0.1). Subsequently, we assigned
736 molecular cell stage labels to each cluster based on the expression of (a) known
737 marker genes for ICM and TF (e.g. FN1, KDM2B for ICM, GATA3 for trophectoderm,
738 etc.(Nagatomo et al., 2013; Negrón-Pérez et al., 2017)); (b) genes first expressed at
739 4-cell stage (minor EGA) or 8-16 cell stage (major EGA) in bovine embryos (Graf et al.,
740 2014). For trajectory analysis, we employed the R package Slingshot (v2.10.0) to infer
741 developmental trajectories based on transcriptome profiles.

742 *Regulon analysis*

743 Regulon analysis was performed on the transcriptome data using pySCENIC
744 (v0.12.1)(Van de Sande et al., 2020). First, for each motif in the public collection
745 (https://resources.aertslab.org/cistarget/motif_collections/), genes in the bovine

746 reference genome bosTau9 (ARS-UCD1.2) with orthologs in humans were prioritized.
747 This prioritization was determined by a scoring system that assessed the presence of
748 the motif within a 10kb window upstream and downstream of the transcription start site.
749 Consequently, a motif x gene matrix was generated. Next, this matrix served as input
750 alongside the raw count matrix to pySCENIC (v0.12.1) to detect active regulons.
751 pySCENIC was run ten separate times, and only regulons appearing two or more times
752 were retained. The final AUC matrix was constructed using the maximum AUC values
753 for each regulon among all runs in which they were present. The AUC heatmap was
754 created with AUC values scaled for each regulon. To rank the identified regulons
755 according to their specificity in each cell lineage, a regulon specificity score was
756 calculated using "calcRSS" function within R package SCENIC (v 1.3.1). To identify the
757 key regulons for each molecular stage, we considered only regulons where
758 corresponding TFs were expressed in more than 50% of the cells. From these, for
759 each stage, we selected the top 6 regulons with the most frequent TF expression
760 among those ranked in the top 20 for both activity and specificity.

761 *Differential expression and regulon analysis*

762 Differential expression analysis was performed by comparing
763 androgenetic/gynogenetic/polyploid cells to biparental diploid cells within each
764 molecular cell stage using the FindMarkers function in Seurat (v5.0.1), employing the
765 "MAST" method with a minimum percentage threshold of 0.5. Pseudotime values and
766 aneuploid status were incorporated as latent variables in the model. Genes were
767 considered differentially expressed if they met the criteria of an adjusted p-value < 0.05

768 and an absolute log2 fold change greater than 1. Differential regulon analysis was
769 performed between cells exhibiting WG abnormalities and biparental diploid cells
770 within each molecular cell stage by Wilcoxon ranked-sum test on the AUC values.
771 Regulons were considered to have significantly different activity if they demonstrated
772 an adjusted *p*-value < 0.05 and an absolute log2 fold change greater than 1. The
773 functions of the differentially expressed genes and regulons were curated through
774 manual online searches and literature reviews.

775 *Statistical analysis*

776 Categorical data were compared using the chi-squared test, with Fisher's exact test
777 applied when cell counts were too small. Pseudotime values were compared using the
778 t-test. Statistical significance was determined using a two-tailed approach with a
779 significance threshold of $p < 0.05$. All tests were conducted in R (v4.3.2).

780 **Data availability**

781 The GBS and single-cell RNA sequencing data reported in this paper are available at
782 the European Nucleotide Archive (ENA) under project number PRJEB76932
783 (https://www.ebi.ac.uk/ena/browser/view/PRJEB76932).

784 **Acknowledgements**

785 Funding was received from the Marie Skłodowska-Curie grant agreement No 813707
786 (MATER) and from the KU Leuven, C1-C14/22/125 to J.R.V. and T.V. T.L. and T.V. were
787 supported by the Research Foundation Flanders (FWO: G0C6120N, G088621N and
788 I001818N). Y.Z. was supported by the Marie Skłodowska-Curie grant agreement No

813707 (MATER). A.F. is supported by the European Union's Horizon 2020 research and innovation programme under the Marie Skłodowska-Curie grant agreement No 860960 and BOF22/ITN/036.

Competing interests

T.V. and J.R.V. are co-inventors on licensed patents WO/2011/157846 (Methods for haplotyping single cells), WO/2014/053664 (High-throughput genotyping by sequencing low amounts of genetic material) and WO/2015/028576 (Haplotyping and copy number typing using polymorphic variant allelic frequencies).

References

Anders S, Pyl PT, Huber W. 2015. HTSeq—a Python framework to work with high-throughput sequencing data. *Bioinformatics* **31**:166. doi:10.1093/BIOINFORMATICS/BTU638

Bakshi A, Iturra FE, Alamban A, Rosas-Salvans M, Dumont S, Aydogan MG. 2023. Cytoplasmic division cycles without the nucleus and mitotic CDK/cyclin complexes. *Cell* **186**:4694-4709.e16. doi:10.1016/J.CELL.2023.09.010/ATTACHMENT/CD4A0F61-45ED-48F1-B6DD-C5F5C35AA432/MMC3

Balaban B, Brison D, Calderón G, Catt J, Conaghan J, Cowan L, Ebner T, Gardner D, Hardarson T, Lundin K, Cristina Magli M, Mortimer D, Mortimer S, Munné S, Royere D, Scott L, Smitz J, Thornhill A, Van Blerkom J, Van Den Abbeel E. 2011. The Istanbul consensus workshop on embryo assessment: proceedings of an expert meeting. *Human Reproduction* **26**:1270–1283. doi:10.1093/HUMREP/DER037

Caroselli S, Figliuzzi M, Picchetta L, Cogo F, Zambon P, Pergher I, Girardi L, Patassini C, Poli M, Bakalova D, Cimadomo D, Findikli N, Coban O, Serdarogullari M, Favero F, Bortolato S, Anastasi A, Capodanno F, Gallinelli A, Brancati F, Rienzi L, Ubaldi FM, Jimenez-Almazán J, Blesa-Jarque D, Miravet-Valenciano J, Rubio C, Simòn C, Capalbo A. 2023. Improved clinical utility of preimplantation genetic testing through the integration of ploidy and common pathogenic microdeletions analyses. *Human Reproduction* **38**:762–775. doi:10.1093/HUMREP/DEAD033

Chatzimeletiou K, Morrison EE, Prapas N, Prapas Y, Handyside AH. 2005. Spindle abnormalities in normally developing and arrested human preimplantation embryos in vitro identified by confocal laser scanning microscopy. *Human Reproduction* **20**:672–682. doi:10.1093/HUMREP/DEH652

Chen S, Zhou Y, Chen Y, Gu J. 2018. fastp: an ultra-fast all-in-one FASTQ preprocessor.

Bioinformatics **34**:i884–i890. doi:10.1093/BIOINFORMATICS/BTY560

Coonen E, Rubio C, Christopikou Di, DImitriadou E, Gontar J, Goossens V, Maurer M, Spinella F, Vermeulen N, De Rycke M. 2020. ESHRE PGT Consortium good practice recommendations for the detection of structural and numerical chromosomal aberrations. *Hum Reprod Open* **2020**:1–20. doi:10.1093/HROPEN/HOAA017

Daughtry BL, Rosenkrantz JL, Lazar NH, Fei SS, Redmayne N, Torkenczy KA, Adey A, Yan M, Gao L, Park B, Nevonen KA, Carbone L, Chavez SL. 2019. Single-cell sequencing of primate preimplantation embryos reveals chromosome elimination via cellular fragmentation and blastomere exclusion. *Genome Res* **29**:367–382. doi:10.1101/GR.239830.118

De Coster T, Masset H, Tšuiko O, Catteeuw M, Zhao Y, Dierckxsens N, Aparicio AL, Dimitriadou E, Debrock S, Peeraer K, de Ruijter-Villani M, Smits K, Van Soom A, Vermeesch JR. 2022. Parental genomes segregate into distinct blastomeres during multipolar zygotic divisions leading to mixoploid and chimeric blastocysts. *Genome Biology 2022 23:1* **23**:1–29. doi:10.1186/S13059-022-02763-2

Deng Q, Huang S. 2004. PRDM5 is silenced in human cancers and has growth suppressive activities. *Oncogene 2004 23:28* **23**:4903–4910. doi:10.1038/sj.onc.1207615

Destouni A, Esteki MZ, Catteeuw M, Tšuiko O, Dimitriadou E, Smits K, Kurg A, Salumets A, Van Soom A, Voet T, Vermeesch JR. 2016. Zygotes segregate entire parental genomes in distinct blastomere lineages causing cleavage-stage chimerism and mixoploidy. *Genome Res* **26**:567–578. doi:10.1101/GR.200527.115

Dobin A, Davis CA, Schlesinger F, Drenkow J, Zaleski C, Jha S, Batut P, Chaisson M, Gingeras TR. 2013. STAR: ultrafast universal RNA-seq aligner. *Bioinformatics* **29**:15–21. doi:10.1093/BIOINFORMATICS/BTS635

Dunn HO, McEntee K, Hansel W. 1970. Diploid-triploid chimerism in a bovine true hermaphrodite. *Cytogenet Genome Res* **9**:245–259. doi:10.1159/000130095

Fernandez Gallardo E, Sifrim A, Chappell J, Demeulemeester J, Herrmann JC, Vermotte R, Kerremans A, Van Der Haegen M, Herck J Van, Vanuytven S, Vandereyken K, Macaulay IC, Vermeesch JR, Peeraer K, Debrock S, Pasque V, Voet T, Affiliations #. 2023. A multi-omics genome-and-transcriptome single-cell atlas of human preimplantation embryogenesis reveals the cellular and molecular impact of chromosome instability. *bioRxiv* 2023.03.08.530586. doi:10.1101/2023.03.08.530586

Fragouli E, Alfarawati S, Spath K, Jaroudi S, Sarasa J, Enciso M, Wells D. 2013. The origin and impact of embryonic aneuploidy. *Hum Genet* **132**:1001–1013. doi:10.1007/S00439-013-1309-0/TABLES/4

Garrison E, Marth G. 2012. Haplotype-based variant detection from short-read sequencing.

Gerri C, McCarthy A, Alanis-Lobato G, Demtschenko A, Bruneau A, Loubersac S, Fogarty NME, Hampshire D, Elder K, Snell P, Christie L, David L, Van de Velde H, Fouladi-Nashta AA, Niakan KK. 2020. Initiation of a conserved trophectoderm program in human, cow and mouse embryos. *Nature 2020 587:7834* **587**:443–447. doi:10.1038/s41586-020-2759-x

Graf A, Krebs S, Zakhartchenko V, Schwalb B, Blum H, Wolf E. 2014. Fine mapping of genome activation in bovine embryos by RNA sequencing. *Proc Natl Acad Sci U S A* **111**:4139–4144. doi:10.1073/PNAS.1321569111/-/DCSUPPLEMENTAL/PNAS.201321569SI.PDF

Hansen PJ. 2010. Medawar redux - an overview on the use of farm animal models to elucidate

principles of reproductive immunology. *Am J Reprod Immunol* **64**:225–230. doi:10.1111/J.1600-0897.2010.00900.X

Hao Y, Lai L, Mao J, Im GS, Bonk A, Prather RS. 2004. Apoptosis in Parthenogenetic Preimplantation Porcine Embryos. *Biol Reprod* **70**:1644–1649. doi:10.1095/BIOLREPROD.103.026005

Hao Y, Stuart T, Kowalski MH, Choudhary S, Hoffman P, Hartman A, Srivastava A, Molla G, Madad S, Fernandez-Granda C, Satija R. 2023. Dictionary learning for integrative, multimodal and scalable single-cell analysis. *Nature Biotechnology 2023 42:2* **42**:293–304. doi:10.1038/s41587-023-01767-y

Hardy K, Handyside AH, Winston RML. 1989. The human blastocyst: cell number, death and allocation during late preimplantation development in vitro. *Development* **107**:597–604. doi:10.1242/DEV.107.3.597

Hardy K, Winston RML, Handyside AH. 1993. Binucleate blastomeres in preimplantation human embryos in vitro: failure of cytokinesis during early cleavage. *Reproduction* **98**:549–558. doi:10.1530/JRF.0.0980549

Hassold T, Chen N, Funkhouser J, Jooss T, Manuel B, Matsuura J, Matsuyama A, Wilson C, Yamane JA, Jacobs PA. 1980. A cytogenetic study of 1000 spontaneous abortions. *Ann Hum Genet* **44**:151–164. doi:10.1111/J.1469-1809.1980.TB00955.X

Hassold T, Hunt P. 2001. To err (meiotically) is human: the genesis of human aneuploidy. *Nature Reviews Genetics 2001 2:4* **2**:280–291. doi:10.1038/35066065

Home P, Kumar RP, Ganguly A, Saha B, Milano-Foster J, Bhattacharya B, Ray S, Gunewardena S, Paul A, Camper SA, Fields PE, Paul S. 2017. Genetic redundancy of GATA factors in the extraembryonic trophoblast lineage ensures the progression of preimplantation and postimplantation mammalian development. *Development (Cambridge)* **144**:876–888. doi:10.1242/DEV.145318/264332/AM/GENETIC-REDUNDANCY-OF-GATA-FACTORS-IN

Hoppe PC, Illmensee K. 1977. Microsurgically produced homozygous-diploid uniparental mice. *Proceedings of the National Academy of Sciences* **74**:5657–5661. doi:10.1073/PNAS.74.12.5657

Hwang IS, Park MR, Lee HS, Kwak TU, Son HY, Kang JK, Lee JW, Lee K, Park EW, Hwang S. 2020. Developmental and Degenerative Characterization of Porcine Parthenogenetic Fetuses during Early Pregnancy. *Animals 2020, Vol 10, Page 622* **10**:622. doi:10.3390/ANI10040622

Ito M, Kaneko-Ishino T, Ishino F, Matsuhashi M, Yokoyama M, Katsuki M. 1991. Fate of haploid parthenogenetic cells in mouse chimeras during development. *Journal of Experimental Zoology* **257**:178–183. doi:10.1002/JEZ.1402570206

Johnson WH, Loskutoff NM, Plante Y, Betteridge KJ. 1995. Production of four identical calves by the separation of blastomeres from an in vitro derived four-cell embryo. *Vet Rec* **137**:15–16. doi:10.1136/VR.137.1.15

Kola I, Trounson A, Dawson G, Rogers P. 1987. Tripronuclear human oocytes: altered cleavage patterns and subsequent karyotypic analysis of embryos. *Biol Reprod* **37**:395–401. doi:10.1095/BIOLREPROD37.2.395

Leng L, Ouyang Q, Kong X, Gong F, Lu C, Zhao L, Shi Y, Cheng D, Hu L, Lu G, Lin G. 2017. Self-diploidization of human haploid parthenogenetic embryos through the Rho

pathway regulates endomitosis and failed cytokinesis. *Scientific Reports 2017 7:1* **7**:1–10. doi:10.1038/s41598-017-04602-y

Leng L, Sun J, Huang J, Gong F, Yang L, Zhang S, Yuan X, Fang F, Xu X, Luo Y, Bolund L, Peters BA, Lu G, Jiang T, Xu F, Lin G. 2019. Single-Cell Transcriptome Analysis of Uniparental Embryos Reveals Parent-of-Origin Effects on Human Preimplantation Development. *Cell Stem Cell* **25**:697-712.e6. doi:10.1016/j.stem.2019.09.004

Li H. 2013. Aligning sequence reads, clone sequences and assembly contigs with BWA-MEM. *arXiv: Genomics*. doi:10.6084/M9.FIGSHARE.963153.V1

Liu D. 2019. Algorithms for efficiently collapsing reads with Unique Molecular Identifiers. *PeerJ* **7**. doi:10.7717/PEERJ.8275

Liu L, Trimarchi JR, Keefe DL. 2002. Haploidy but Not Parthenogenetic Activation Leads to Increased Incidence of Apoptosis in Mouse Embryos. *Biol Reprod* **66**:204–210. doi:10.1095/BIOLREPROD66.1.204

López-Maury L, Marguerat S, Bähler J. 2008. Tuning gene expression to changing environments: from rapid responses to evolutionary adaptation. *Nature Reviews Genetics 2008 9:8* **9**:583–593. doi:10.1038/nrg2398

Lucifero D, Suzuki J, Bordignon V, Martel J, Vigneault C, Therrien J, Filion F, Smith LC, Trasler JM. 2006. Bovine SNRPN Methylation Imprint in Oocytes and Day 17 In Vitro-Produced and Somatic Cell Nuclear Transfer Embryos. *Biol Reprod* **75**:531–538. doi:10.1095/BIOLREPROD.106.051722

Ma LB, Yang L, Zhang Y, Cao JW, Hua S, Li JX. 2008. Quantitative analysis of mitochondrial RNA in goat–sheep cloned embryos. *Mol Reprod Dev* **75**:33–39. doi:10.1002/MRD.20736

Macaulay IC, Teng MJ, Haerty W, Kumar P, Ponting CP, Voet T. 2016. Separation and parallel sequencing of the genomes and transcriptomes of single cells using G&T-seq. *Nature Protocols 2016 11:11* **11**:2081–2103. doi:10.1038/nprot.2016.138

Madan K. 2020. Natural human chimeras: A review. *Eur J Med Genet* **63**:103971. doi:10.1016/J.EJMG.2020.103971

Marsico TV, Valente RS, Annes K, Oliveira AM, Silva MV, Sudano MJ. 2023. Species-specific molecular differentiation of embryonic inner cell mass and trophectoderm: A systematic review. *Anim Reprod Sci* **252**:107229. doi:10.1016/J.ANIREPROSCI.2023.107229

Martin M. 2011. Cutadapt removes adapter sequences from high-throughput sequencing reads. *EMBnet J* **17**:10–12. doi:10.14806/EJ.17.1.200

Masset H, Ding J, Dimitriadou E, Debrock S, Tšuiko O, Smits K, Peeraer K, Voet T, Esteki MZ, Vermeesch JR. 2022. Single-cell genome-wide concurrent haplotyping and copy-number profiling through genotyping-by-sequencing. *Nucleic Acids Res* **50**:e63–e63. doi:10.1093/NAR/GKAC134

Masset H, Tšuiko O, Vermeesch JR. 2021. Genome-wide abnormalities in embryos: Origins and clinical consequences. *Prenat Diagn* **41**:554–563. doi:10.1002/PD.5895

May-Panloup P, Vignon X, Chrétien MF, Heyman Y, Tamassia M, Mathièry Y, Reynier P. 2005. Increase of mitochondrial DNA content and transcripts in early bovine embryogenesis associated with upregulation of mtTFA and NRF1 transcription factors. *Reproductive Biology and Endocrinology* **3**:1–8. doi:10.1186/1477-7827-3-65/FIGURES/3

McCoy RC, Demko ZP, Ryan A, Banjevic M, Hill M, Sigurjonsson S, Rabinowitz M, Petrov DA.

954 2015. Evidence of Selection against Complex Mitotic-Origin Aneuploidy during
955 Preimplantation Development. *PLoS Genet* **11**. doi:10.1371/JOURNAL.PGEN.1005601
956 Meinecke B, Kuiper H, Drögemüller C, Leeb T, Meinecke-Tillman S. 2003. A Mola Hydatidosa
957 Coexistent with a Foetus in a Bovine Freemartin Pregnancy. *Placenta* **24**:107–112.
958 doi:10.1053/PLAC.2002.0872
959 Nagatomo H, Kagawa S, Kishi Y, Takuma T, Sada A, Yamanaka K ichi, Abe Y, Wada Y, Takahashi
960 M, Kono T, Kawahara M. 2013. Transcriptional Wiring for Establishing Cell Lineage
961 Specification at the Blastocyst Stage in Cattle1. *Biol Reprod* **88**:158–159.
962 doi:10.1095/BIOLREPROD.113.108993/2514370
963 Negrón-Pérez VM, Zhang Y, Hansen PJ. 2017. Single-cell gene expression of the bovine
964 blastocyst. *Reproduction* **154**:627–644. doi:10.1530/REP-17-0345
965 Niakan KK, Eggan K. 2013. Analysis of human embryos from zygote to blastocyst reveals
966 distinct gene expression patterns relative to the mouse. *Dev Biol* **375**:54–64.
967 doi:10.1016/J.YDBIO.2012.12.008
968 Ottolini CS, Kitchen J, Xanthopoulou L, Gordon T, Summers MC, Handyside AH. 2017. Tripolar
969 mitosis and partitioning of the genome arrests human preimplantation development in
970 vitro. *Scientific Reports 2017 7:1* **7**:1–10. doi:10.1038/s41598-017-09693-1
971 Santos RR, Schoevers EJ, Roelen BAJ. 2014. Usefulness of bovine and porcine IVM/IVF models
972 for reproductive toxicology. *Reprod Biol Endocrinol* **12**:1–12. doi:10.1186/1477-7827-
973 12-117
974 Seckl MJ, Sebire NJ, Berkowitz RS. 2010. Gestational trophoblastic disease. *The Lancet*
975 **376**:717–729. doi:10.1016/S0140-6736(10)60280-2
976 Sherard J, Bean C, Bove B, DelDuca V, Esterly KL, Karcsh HJ, Munshi G, Reamer JF, Suazo G,
977 Wilmoth D. 1986. Long survival in a 69,XXY triploid male. *Am J Med Genet* **25**:307–312.
978 doi:10.1002/AJMG.1320250216
979 Shu X sheng, Geng H, Li L, Ying J, Ma C, Wang Y, Poon FF, Wang X, Ying Y, Yeo W, Srivastava
980 G, Tsao SW, Yu J, Sung JJY, Huang S, Chan ATC, Tao Q. 2011. The Epigenetic Modifier
981 PRDM5 Functions as a Tumor Suppressor through Modulating WNT/β-Catenin
982 Signaling and Is Frequently Silenced in Multiple Tumors. *PLoS One* **6**:e27346.
983 doi:10.1371/JOURNAL.PONE.0027346
984 Sigalos G, Triantafyllidou O, Vlahos NF. 2016. Novel embryo selection techniques to increase
985 embryo implantation in IVF attempts. *Arch Gynecol Obstet* **294**:1117–1124.
986 doi:10.1007/S00404-016-4196-5/TABLES/1
987 Sugimura S, Akai T, Hashiyada Y, Somfai T, Inaba Y, Hirayama M, Yamanouchi T, Matsuda H,
988 Kobayashi S, Aikawa Y, Ohtake M, Kobayashi E, Konishi K, Imai K. 2012. Promising System
989 for Selecting Healthy In Vitro–Fertilized Embryos in Cattle. *PLoS One* **7**:e36627.
990 doi:10.1371/JOURNAL.PONE.0036627
991 Sugimura S, Akai T, Imai K. 2017. Selection of viable in vitro-fertilized bovine embryos using
992 time-lapse monitoring in microwell culture dishes. *Journal of Reproduction and*
993 *Development* **63**:353–357. doi:10.1262/JRD.2017-041
994 Tarkowski AK. 1977. In vitro development of haploid mouse embryos produced by bisection
995 of one-cell fertilized eggs. *Development* **38**:187–202. doi:10.1242/DEV.38.1.187
996 Thundathil J, Filion F, Smith LC. 2005. Molecular control of mitochondrial function in
997 preimplantation mouse embryos. *Mol Reprod Dev* **71**:405–413. doi:10.1002/MRD.20260

Tšuiko O, Catteeuw M, Esteki MZ, Destouni A, Pascottini OB, Besenfelder U, Havlicek V, Smits K, Kurg A, Salumets A, D'Hooghe T, Voet T, Van Soom A, Vermeesch JR. 2017. Genome stability of bovine in vivo-conceived cleavage-stage embryos is higher compared to in vitro-produced embryos. *Human Reproduction* **32**:2348–2357. doi:10.1093/HUMREP/DEX286

Tšuiko O, Vanneste M, Melotte C, Ding J, Debrock S, Masset H, Peters M, Salumets A, De Leener A, Pirard C, Kluyskens C, Hostens K, van de Vijver A, Peeraer K, Denayer E, Vermeesch JR, Dimitriadou E. 2021. Haplotyping-based preimplantation genetic testing reveals parent-of-origin specific mechanisms of aneuploidy formation. *NPJ Genom Med* **6**. doi:10.1038/S41525-021-00246-0

Van de Sande B, Flerin C, Davie K, De Waegeneer M, Hulselmans G, Aibar S, Seurinck R, Saelens W, Cannoodt R, Rouchon Q, Verbeiren T, De Maeyer D, Reumers J, Saeys Y, Aerts S. 2020. A scalable SCENIC workflow for single-cell gene regulatory network analysis. *Nature Protocols 2020 15:7* **15**:2247–2276. doi:10.1038/s41596-020-0336-2

Vanneste E, Voet T, Le Caignec C, Ampe M, Konings P, Melotte C, Debrock S, Amyere M, Vikkula M, Schuit F, Fryns JP, Verbeke G, D'Hooghe T, Moreau Y, Vermeesch JR. 2009. Chromosome instability is common in human cleavage-stage embryos. *Nature Medicine 2009 15:5* **15**:577–583. doi:10.1038/nm.1924

Willadsen SM. 1980. The viability of early cleavage stages containing half the normal number of blastomeres in the sheep. *Reproduction* **59**:357–362. doi:10.1530/JRF.0.0590357

Wydooghe E, Vaele L, Piepers S, Dewulf J, Van Abbeel E Den, De Sutter P, Van Soom A. 2014. Individual commitment to a group effect: strengths and weaknesses of bovine embryo group culture. *Reproduction* **148**:519–529. doi:10.1530/REP-14-0213

Xu J, Shu Y, Yao G, Zhang Yu, Niu W, Zhang Yile, Ma X, Jin H, Zhang F, Shi S, Wang Y, Song W, Dai S, Cheng L, Zhang X, Xie W, Hsueh AJ, Sun Y. 2021. Parental methylome reprogramming in human uniparental blastocysts reveals germline memory transition. *Genome Res* **31**:1519. doi:10.1101/GR.273318.120/-/DC1

Zamani Esteki M, Dimitriadou E, Mateiu L, Melotte C, Van der Aa N, Kumar P, Das R, Theunis K, Cheng J, Legius E, Moreau Y, Debrock S, D'Hooghe T, Verdyck P, De Rycke M, Sermon K, Vermeesch JR, Voet T. 2015. Concurrent Whole-Genome Haplotyping and Copy-Number Profiling of Single Cells. *Am J Hum Genet* **96**:894. doi:10.1016/J.AJHG.2015.04.011

Zaragoza M V., Surti U, Redline RW, Millie E, Chakravarti A, Hassold TJ. 2000. Parental origin and phenotype of triploidy in spontaneous abortions: Predominance of diandry and association with the partial hydatidiform mole. *Am J Hum Genet* **66**:1807–1820. doi:10.1086/302951

Zhan Q, Ye Z, Clarke R, Rosenwaks Z, Zaninovic N. 2016. Direct Unequal Cleavages: Embryo Developmental Competence, Genetic Constitution and Clinical Outcome. *PLoS One* **11**:e0166398. doi:10.1371/JOURNAL.PONE.0166398